Scission Deformation of the $^{120}Cd/^{132}Sn$ Neutronless Fragmentation in $^{252}Cf(sf)$

A. Francheteau,[1,2] L. Gaudefroy,[1,2] G. Scamps,[3] O. Roig,[1,2] V. Méot,[1,2] A. Ebran,[1] and G. Bélier[1,2]
[1]*CEA, DAM, DIF, 91297 Arpajon, France*
[2]*Université Paris-Saclay, CEA, Laboratoire Matière en Conditions Extrêmes, 91680 Bruyères-le-Châtel, France*
[3]*Laboratoire des 2 Infinis—Toulouse (L2IT-IN2P3), Université de Toulouse, CNRS, UPS, F-31062 Toulouse Cedex 9, France*

(Received 22 December 2023; accepted 29 February 2024; published 3 April 2024)

We report on a study of the radiative decay of fission fragments populated via neutronless fission of $^{252}Cf(sf)$. Applying the double-energy method a perfect mass identification is achieved for these rare events. In the specific case of the $^{120}Cd/^{132}Sn$ cold fragmentation, we find that ^{132}Sn is produced in its ground state. We can therefore directly measure the excitation energy of the complementary fragment, ^{120}Cd. The reproduction of the γ-ray spectrum, measured in coincidence with the neutronless fission events, is sensitive to the angular momentum distribution of the studied primary fragment. The latter estimated using a time-dependent collective Hamiltonian model, allows us to constrain for the first time the deformation ($\beta_2 \simeq 0.4$) of the studied fission fragment at scission. The present work demonstrates the high potential of the understudied neutronless fission channel for extracting detailed information on both fission fragments and process.

DOI: 10.1103/PhysRevLett.132.142501

Nuclear fission, known for eighty-five years [1,2], is a dynamical many-body quantum problem where both single-particle and collective effects involving the underlying constituents of the nucleus are at play. As such, fission remains one of the most difficult processes to model in nuclear physics [3]. Experimentally, fission is also a challenging subject to address as it produces a large number of pairs of highly excited and deformed fragments decaying through neutron and gamma emission.

Fission studies have known a revival in the last 10 years on both theoretical and experimental sides, thanks to the development of high-performance detection systems [4] and a large increase in computational resources [5]. Open questions remain on the deformation of the primary fragments [6,7]; the mechanism at the origin of their angular momentum [8–12], and the excitation energy sharing between fission fragments [13,14]. Because of its capital importance for applications, neutron emission in fission has been the subject of numerous studies [15] and remains the experimental quantity of choice for constraining excitation energy of the fission fragments [16,17]. Angular momentum is often addressed via the study of the γ decay of the fragments [8,18]. A particular class of fission events greatly simplifies the identification of fission fragments identification and subsequently the data interpretation: fission without neutron emission [19–22]. In that case, momentum conservation directly links the kinetic energy of the fragments to their masses. In the absence of neutron emission, the γ quanta are responsible for both excitation energy and angular momentum removal. Therefore, the combined measurement of kinetic energies and γ-ray emission in neutronless fission is a way to explore these topics and constrain or test models. The high selectivity achievable in neutronless fission experiments might counteract its low probability of occurrence, making it a tool of interest also for nuclear structure studies [23]. The present Letter reports on the radiative decay of the $^{120}Cd/^{132}Sn$ neutronless fragmentation populated in the spontaneous fission of ^{252}Cf. This cold fragmentation is an exceptional case where the doubly magic nucleus ^{132}Sn is in its ground state (GS) making it possible to extract detailed experimental information, such as excitation energy distribution or total γ-ray spectrum, unambiguously associated with the light fragment. Our results, interpreted within a time-dependent collective Hamiltonian approach, allow us to access the angular momentum distribution of the fragments as well as their deformations at scission. These results might also have far reaching consequences for application purposes such as γ heating in nuclear reactors.

The double-energy method [24] was used in order to identify in mass the fragments produced in the neutronless channel of the spontaneous fission of ^{252}Cf. We used a twin Frisch-grid ionization chamber (TFGIC). The detector was loaded with a ^{252}Cf source of 1.35 kBq activity, deposited on an ultrathin carbon backing (5 $\mu g\,cm^{-2}$), prepared using the self-transfer technique [25]. The design of the TFGIC is inspired by our previous work [26] with the additional constraint that it had to fit at the center of a nearly $4\pi\gamma$ array. A brief description of the experimental setup is as follows. The TFGIC is a 135 mm long, 162 mm outer diameter axially symmetrical gaseous detector. It consists of two identical ionization chambers mounted back-to-back and sharing a common cathode at the center, defining a plane of

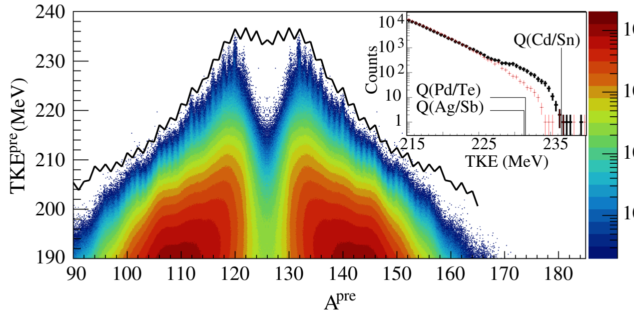

FIG. 1. Total kinetic energy versus the mass of the fragment, before neutron emission. The black line in the extreme TKE part of the figure shows the largest Q value for a given mass fragmentation. The inset shows the high energy part of the TKE distribution gated by the mass ratio 120/132 (black) compared with the neighboring mass 119/133 distribution (red). Q values for the most energetic isotopic fragmentations with $A_L/A_H = 120/132$ are shown.

symmetry of the detector. The ^{252}Cf sample was held at the center of the cathode. The anodes are placed 31 mm apart from the cathode. A Frisch grid, consisting in a 88% transparency wire mesh, is interposed between the cathode and the anode, 25 mm apart from the cathode. For this measurement, the grid was grounded while the cathode was set at -1800 V and the anode at 1500 V. The TFGIC was operated with a P10 gas mixture (90% Ar + 10% CH4) at 1.5 bars continuously flowing through the chamber at a rate of 0.1 L min^{-1}. At the working pressure, the typical range for the fission fragments of ^{252}Cf amounts to 15 mm. An energy resolution of about 35 keV (FWHM) of the TFGIC was measured prior to the fission run using a standard 3α source.

The TFGIC was located at the center of an array composed of 54 identical NaI-Tl γ detectors. The NaI crystals present a 102×102 mm^2 basis and a 152 mm height. They are encapsulated in an Al housing, with a 1 mm thickness for the entrance window and 1.5 mm for the other faces. The detectors were arranged in a cubic geometry, the faces of which were composed of nine detectors. The geometrical efficiency of the γ array amounts to 92%. GEANT4 [27] simulations of the γ array have been performed in order to obtain its response function in a matrix form. These simulations have been validated against measured γ-ray spectra obtained with calibrated sources of ^{22}Na, ^{152}Eu, and ^{207}Bi. The simulations also account for the energy resolution of the detection system, determined with the γ sources, and for the mean Doppler effect (energy broadening) for the studied fission fragments. Energy calibration of the array was performed from 59 keV up to 2614 keV using standard γ sources and some typical γ lines from room background. The linearity was checked up to 4.4 MeV using an AmBe source. The time resolution of the NaI detectors was measured to be about 5.5 ns (FWHM).

Details on the analysis procedure can be found in Ref. [28] and will be the subject of a future article [29]. Here we recall its main steps. The desired primary mass of the fragment, m, is linked to the preneutron emission energies, E, by the relation $m_{L,H} = 252[E_{H,L}/(E_L + E_H)]$, where the indices stand for the light and heavy fragments. However, only postneutron energies are measured. A well-documented iterative procedure [26,30] allows us to access preneutron energies and to reconstruct the primary masses. It accounts for (i) energy loss of the fragments in the backing of the source; (ii) the fragment pulse height defect (PHD) in the gas, and (iii) the energy correction due to neutron emission. The preneutron energy is linked to the postneutron energy, E^*, by the relation $E = E^*\{m/[m - \nu(m, \mathrm{TKE})]\}$. The number, $\nu(m, \mathrm{TKE})$, of neutrons emitted by a fragment of mass, m, in a fission event of total kinetic energy, TKE, is estimated following the prescription proposed in Ref. [31]. This correction vanishes for neutronless events. The parameterization of the PHD correction is adopted from Ref. [32] and adjusted so as to reproduce the data from Ref. [33]. For the energy-loss correction, the angle between the fission axis and the symmetry axis of the chamber is needed. It is reconstructed for each fragment using the time difference between the signal of each anode and that of the cathode [34]. Despite our efforts, this procedure ends up in a slightly anisotropic distribution of the fission fragments, as previously observed in Ref. [26]. This defect is found not to affect the rest of the data, and the present standard quantities, such as mean masses, kinetic energies, or associated widths, are in good agreement with literature values [28,29].

Figure 1 shows the high energy part of the preneutron TKE distribution measured in this work as a function of the deduced preneutron mass of the fragments. The vertical lines observed for the most energetic fragmentations correspond to fission events for which both fragments are populated below their neutron separation energies. For these rare neutronless events (about 2.10^{-3} of the events for ^{252}Cf [35]), we determined an excellent mass resolution of 0.68 amu, FWHM. The black line in Fig. 1 indicates the largest Q value for the primary fragmentation A_L/A_H, $Q_{\max}$, calculated using the tabulated masses [36]. As observed in previous works [21,22], the TKE distribution in Fig. 1 almost never reaches $Q_{\max}$ except for the 120/132 fragmentation where $Q_{\max}$ is obtained for $Z_L/Z_H = 48/50$. The high energy part of the experimental TKE distribution for this mass split is shown in the inset of Fig. 1, where it is compared to the distribution of the neighboring mass split. The $Q_{\max}^{Z_H=50,51,52}$ values, for $A_H = 132$, are also shown in the inset. One sees that only the ^{120}Cd/^{132}Sn fragmentation contributes to the last 5 MeV of the TKE distribution, and is responsible for the clear shoulder observed in the TKE distribution contrasting with that of the neighboring split.

Figure 2(a) shows the low energy part of the γ spectrum measured in prompt coincidence ($\Delta T = \pm 4$ ns) with the last 8 MeV [$S_n(^{120}\mathrm{Cd}) = 8.05$ MeV] of the TKE

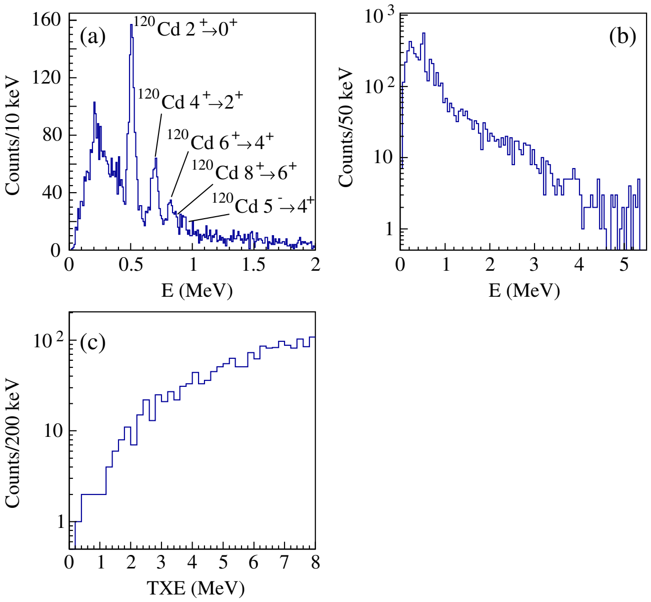

FIG. 2. (a) Low energy part of the γ-ray spectrum measured in coincidence with the last 8 MeV of the TKE distribution of the 120/132 mass split. (b) Same as (a) for the entire spectrum. (c) Total excitation energy distribution, TXE $= Q - $ TKE, for the events displayed in (a) and (b).

distribution of the 120/132 mass fragmentation. One clearly recognizes the known low-energy transitions in ^{120}Cd [37]. None of the γ rays originating from other $A = 120$ or $A = 132$ fragments are statistically visible in this spectrum. Figure 2(b) shows the γ spectrum on the entire energy scale. Surprisingly, none of the known γ rays in ^{132}Sn are observed in this spectrum nor in the delayed spectrum. We remind the reader that these γ rays should be looked for above the 2_1^+ excitation energy ($E_{2_1^+} = 4.04$ MeV) for an excited state that decays to the ground state of the nucleus either directly or via the 2_1^+ state. Given the present statistics (1483 selected fission events), the γ-ray efficiency and energy resolution at 4.4 MeV, $\epsilon \simeq 13\%$ and $\sigma \simeq 80$ keV, respectively, we estimate that the heavy fragment, ^{132}Sn, is populated in its ground state in at least 98% of the selected events. In the following, we neglect the excitation of this nucleus. At first, this result might seem surprising. It is, however, well accounted for by various phenomenological models aiming at the description of excitation energy sharing between fission fragments [13,38] because of the pronounced shell effect in ^{132}Sn. The total excitation energy distribution, TXE, determined using the simple relation TXE $= Q - $ TKE, therefore solely corresponds to the excitation energy distribution of ^{120}Cd. It is shown in Fig. 2(c). To the best of our knowledge, this is the first determination of this quantity for a fission fragment.

The γ-ray spectrum shown in Figs. 2(a) or 2(b) is thus solely due to the deexcitation of ^{120}Cd, populated according to the excitation energy distribution shown in Fig. 2(c). In the following, we show that the reproduction of this spectrum allows us to gain further insight into the deformation of the fragment at scission. For that purpose, we developed a Monte Carlo code simulating the γ cascade of the nucleus populated following the measured TXE distribution by calculating the photon transmission coefficient and the photon radiative width. The needed inputs are (i) the knowledge of the discrete level scheme of the nucleus; (ii) a parameterization of the nuclear level density (NLD) and γ-strength function (γSF) in order to account for the γ transitions in the continuum region of the level scheme; and (iii) the angular momentum (AM) distribution of ^{120}Cd after scission. The results of the code are folded with the aforementioned GEANT4 response matrix of the detection system in order to obtain the simulated spectrum. The most complete dataset on the low-lying level scheme of ^{120}Cd comes from the Gammasphere study of the ^{252}Cf fission [37]. Considering their measured level scheme up to 2.6 MeV allows us to provide a good description of the low-energy part of the present gamma spectrum, as shown in the following.

We have studied the dependency of the shape of γ spectrum with the NLD and γSF models used in order to describe the statistical γ decay of ^{120}Cd, above 2.6 MeV. In both cases, we have tested the results of two microscopic mean-field approaches whose results are gathered in the TALYS suite [39]: the Skyrme-HFB model or calculations within the quasi-particle random phase approximation using the D1M Gogny force [40]. We also considered the composite Gilbert Cameron model (CGCM) for the NLD as well as the standard Lorentzian (SLO) form for the γSF. The parameters of the former are taken from TALYS while those of the latter are extrapolated from the experimental data available in the less exotic ^{105,106,111,112}Cd nuclei [41]. As a result, the shape of the γ spectrum is found to be robust and within the reported error bars, no major difference is observed between the various models tested for the NLD and the γSF [28]. In the following, we show results obtained for the CGCM NLD and the SLO γSF. It should be noted that the models do not show large discrepancies between each other and that only relative variations in the NLD or γSF matter. Indeed any difference in normalization is canceled in the expression of the radiative width, since we consider only the γ decay of the fragment populated below its neutron separation energy.

The input with the largest impact on the reproduction of the reported γ-ray spectrum, in particular its low energy part, i.e., the part of highest statistical significance, is the AM distribution of ^{120}Cd. In the following, we briefly describe the theoretical approach used in order to obtain this distribution.

To elucidate the emergence of angular momentum in cold fission, we invoke the orientation-pumping mechanism [42]. We consider deformed fragments whose principal deformation axis forms an angle θ_F with the fission axis. In

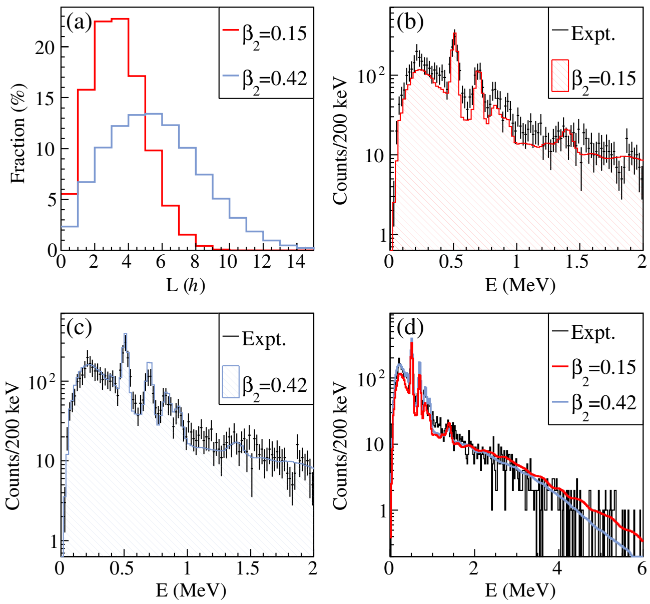

FIG. 3. (a) AM distribution calculated for ^{120}Cd for $\beta_2 = 0.15$ and $\beta_2 = 0.42$. (b) Low energy part of the experimental γ spectrum compared to the simulated one for $\beta_2 = 0.15$. (c) Same as (b) for $\beta_2 = 0.42$. (d) Experimental γ spectrum, compared with the simulated ones for both deformations.

a schematic view, assuming a harmonic potential describing the energy of the two-fragment system as a function of the orientation angles θ_F, the zero point energy is associated with an angle fluctuation expressed as $\sigma^2_{\theta_F} = \hbar/\sqrt{\mu C}$, with μ the moment of inertia of the fragment and C the harmonic potential constant $V(\theta_F) = 1/2C\theta_F^2$. In turn, in line with the Heisenberg principle, the AM of the fragment, i.e., the conjugate variable of the orientation angle, follows the distribution $P(L) = [(2L+1)/\sigma_L]e^{-[L(L+1)/2\sigma_L^2]}$, where $\sigma_L = 1/\sigma_{\theta_F}$ is equivalent to the spin cut-off parameter. This expression is similar to the Bethe distribution [43] but is not due to statistical fluctuations.

Here we use a collective Hamiltonian approach detailed in Ref. [10], with a nucleus-nucleus potential computed with the frozen Hartree-Fock (FHF) assumption [44]. In that approach, both fragments are supposed to be cold and rigid. They are placed in the same lattice at a distance D, and oriented as defined above with respect to the fission axis. The dependence of energy of the system with the angles determines the angular potential responsible for the pumping mechanism. The wave packet is then evolved using the time-dependent Schrödinger equation. After passing the scission point, the model also accounts for the AM generation due to the Coulomb torque. In the present case of the ^{120}Cd/^{132}Sn cold fragmentation, the Sn fragment is assumed to be in its spherical ground state, in line with the above data. The Hartree-Fock calculations are done with the SLY4D functional [45] and the fragments are obtained with the SKY3D code [46].

Two quadrupole deformations, as defined in [10], are tested for the ^{120}Cd fragment; the GS deformation, $\beta_2 = 0.15$, and a larger deformation, $\beta_2 = 0.42$, corresponding to a shoulder in the potential energy curve 4.4 MeV above the GS minimum, compatible with the measured excitation energy distribution. The AM distributions calculated for the two aforementioned quadrupole deformations are compared in Fig. 3(a) while Figs. 3(b) and 3(c) compare the measured γ spectrum below 2 MeV with the simulated ones for both deformation parameters. The AM distribution for $\beta_2 = 0.42$ leads to a much better agreement with the measured data [Fig. 3(c)] than that for the GS deformation, in particular between 750 keV and 1 MeV, for transitions from the high spin states in ^{120}Cd. This is in line with the mean values of the AM distributions shown in Fig. 3(a), $\bar{L} = 3.4\ \hbar$ and $\bar{L} = 5.1\ \hbar$, for $\beta_2 = 0.15$ and $\beta_2 = 0.42$, respectively. It is also worth mentioning that the mean multiplicity of the simulated γ cascades amounts to $\overline{M_\gamma} = 3.5$ and $\overline{M_\gamma} = 4.6$ for $\beta_2 = 0.15$ and $\beta_2 = 0.42$, respectively. This is clearly reflected in the global lower amplitude of the simulated spectrum in Fig. 3(b), as compared to Fig. 3(c). In order to extract the experimental mean γ multiplicity we unfolded the GEANT4 response function of the detection system from our measured spectrum using the Gold's method [47]. The experimental mean γ multiplicity is then the ratio between the integral of the unfolded spectrum and the considered number of fission events. We found $\overline{M}_\gamma^{\text{expt}} = 5.1$ (6), in a close agreement with the simulated multiplicity for $\beta_2 = 0.42$. Notably, this multiplicity closely aligns with that found without excitation energy constraints [48], indicating weak temperature dependence of AM generation. The current fission scenario unveils several facets of the scission dynamics: (i) It affirms the absence of correlations in the generation of AMs, as found in prior works [8,10,49]. (ii) It corresponds to a case where the relative orbital angular momentum $\mathbf{\Lambda}$ is equivalent to the angular momentum of the light fragment. (iii) Given that the $\mathbf{\Lambda}$ vector is inherently perpendicular to the fission axis (z axis), the z component of the AM for the light fragment is zero.

In this Letter, we report on the experimental study of the radiative decay of neutronless fission fragments populated in ^{252}Cf(sf). Applying the 2E-method we achieved a mass resolution of 0.68 amu for neutronless events. Combined with a close to 4π NaI γ array we identified the exceptional neutronless fragmentation ^{120}Cd/^{132}Sn where ^{132}Sn is in its GS, and only ^{120}Cd is excited. For these particular events, we measure the excitation energy distribution of ^{120}Cd. The angular momentum distribution of ^{120}Cd at scission is found to be a key ingredient for the reproduction of the measured γ spectrum. The orientation-pumping mechanism is used in a time-dependent collective Hamiltonian approach in order to extract the angular momentum distribution of the fragment as a function of its deformation. The experimental γ-ray spectrum is well accounted for when considering a quadrupole deformation for ^{120}Cd at scission significantly larger than that calculated for the ground state.

Other results from the present study will follow, in particular on the excitation energy repartition in neutronless fission. In the future, we also plan to combine the present fission detector with a 4π neutron array in order to assess the fission energetics at the opening of the neutron emission channel.

[1] O. Hahn and F. Strassmann, Naturwissenschaften **27**, 11 (1939).
[2] L. Meitner and O. R. Frisch, Nature (London) **143**, 239 (1939).
[3] M. Bender, R. Bernard, G. Bertsch *et al.*, J. Phys. G **47**, 113002 (2020).
[4] A. N. Andreyev, K. Nishio, and K.-H. Schmidt, Rep. Prog. Phys. **81**, 016301 (2018).
[5] N. Schunck and D. Regnier, Prog. Part. Nucl. Phys. **125**, 103963 (2022).
[6] G. Scamps and C. Simenel, Nature (London) **564**, 382 (2018).
[7] A. Bulgac, S. Jin, K. J. Roche, N. Schunck, and I. Stetcu, Phys. Rev. C **100**, 034615 (2019).
[8] J. N. Wilson, D. Thisse, M. Lebois *et al.*, Nature (London) **590**, 566 (2021).
[9] A. Bulgac, I. Abdurrahman, S. Jin, K. Godbey, N. Schunck, and I. Stetcu, Phys. Rev. Lett. **126**, 142502 (2021).
[10] G. Scamps and G. Bertsch, Phys. Rev. C **108**, 034616 (2023).
[11] J. Randrup and R. Vogt, Phys. Rev. Lett. **127**, 062502 (2021).
[12] P Marević, N Schunck, J Randrup, and R Vogt, Phys. Rev. C **104**, L021601 (2021).
[13] K.-H. Schmidt and B. Jurado, Phys. Rev. Lett. **104**, 212501 (2010); Phys. Rev. C **83**, 061601(R) (2011).
[14] A. Bulgac, P. Magierski, K. J. Roche, and I. Stetcu, Phys. Rev. Lett. **116**, 122504 (2016).
[15] V. V. Malinovskij, V. G. Vorob'eva, and B. D. Kuz'minov, AIEA Report No INDC(CCP)–239/L, 1985.
[16] A. A. Naqvi, F. Käppeler, F. Dickmann, and R. Müller, Phys. Rev. C **34**, 218 (1986).
[17] K. Nishio, M. Nakashima, I. Kimura, and Y. Nakagome, J. Nucl. Sci. Technol. **35**, 631 (1998).
[18] J. B. Wilhelmy, E. Cheifetz, R. C. Jared, S. G. Thompson, H. R. Bowman, and J. O. Rasmussen, Phys. Rev. C **5**, 2041 (1972).
[19] W. M. Gibson, T. D. Thomas, and G. L. Miller, Phys. Rev. Lett. **7**, 65 (1961).
[20] J. C. D. Milton and J. S. Fraser, Phys. Rev. Lett. **7**, 67 (1961).
[21] H.-H. Knitter, F.-J. Hambsch, and C. Budtz-Jørgensen, Nucl. Phys. **536A**, 221 (1992).
[22] F. Gönnenwein, A. Möller, M. Cröni *et al.*, Il Nuovo Cimento **110**, 1089 (1997).
[23] L. Gaudefroy, S. Péru, N. Arnal, J. Aupiais, J.-P. Delaroche, M. Girod, and J. Libert, Phys. Rev. C **97**, 064317 (2018).
[24] H. C. Britt, H. E. Wegner, and S. L. Whetstone Jr., Nucl. Instrum. Methods **24**, 13 (1963).
[25] S. Pauker and N. H. Steiger-Shafrir, Nucl. Instrum. Methods **91**, 557 (1971).
[26] L. Gaudefroy, T. Roger, J. Pancin, C. Spitaels, J. Aupiais, and J. Mottier, Nucl. Instrum. Methods Phys. Res., Sect. A **855**, 133 (2017).
[27] S. Agostinelli, J. Allison, K. Amako *et al.*, Nucl. Instrum. Methods Phys. Res., Sect. A **506**, 256 (2003).
[28] A. Francheteau, Ph.D. thesis, Univ. Paris-Saclay, 2023; english version at https://theses.hal.science/tel-04324990.
[29] A. Francheteau, L. Gaudefroy, O. Roig *et al.*, Phys. Rev. C (in preparation).
[30] V. N. Dushin, F.-J. Hambsch, V. A. Jakovlev *et al.*, Nucl. Instrum. Methods Phys. Res., Sect. A **516**, 539 (2004).
[31] G. Barreau, A. Sicre, F. Caïtucoli *et al.*, Nucl. Phys. **A432**, 411 (1985).
[32] F.-J. Hambsch, J. Van-Aarle, and R. Vogt, Nucl. Instrum. Methods Phys. Res., Sect. A **361**, 257 (1995).
[33] M. Peck, A. Göök, J. Enders, F.-J. Hambsch, and S. Oberstedt, Nucl. Instrum. Methods Phys. Res., Sect. A **919**, 105 (2019).
[34] A. Göök, M. Chernykh, J. Enders, A. Oberstedt, and S. Oberstedt, Nucl. Instrum. Methods Phys. Res., Sect. A **621**, 401 (2010).
[35] P. Santi and M. Miller, Nucl. Sci. Eng. **160**, 190 (2008).
[36] G. Audi, F. G. Kondev, M. Wang, B. Pfeiffer, X. Sun, J. Blachot, and M. MacCormick, Chin. Phys. C **36**, 1157 (2012).
[37] Y. X. Luo, J. O. Rasmussen, C. S. Nelson, J. H. Hamilton *et al.*, Nucl. Phys. **A874**, 32 (2012).
[38] O. Litaize, O. Serot, and L. Berge, Eur. Phys. J. A **51**, 77 (2015).
[39] A. Koning, S. Hilaire, and S. Goriely, Eur. Phys. J. A **59**, 131 (2023).
[40] S. Goriely, S. Hilaire, M. Girod, and S. Péru *et al.*, Phys. Rev. Lett. **102**, 242501 (2009).
[41] A. C. Larsen, I. E. Ruud, A. Bürger, S. Goriely *et al.*, Phys. Rev. C **87**, 014319 (2013).
[42] L. Bonneau, P. Quentin, and I. N. Mikhailov, Phys. Rev. C **75**, 064313 (2007).
[43] H. A. Bethe, Phys. Rev. **50**, 332 (1936).
[44] C. Simenel, A. S. Umar, K. Godbey, M. Dasgupta, and D. J. Hinde, Phys. Rev. C **95**, 031601(R) (2017).
[45] K.-H. Kim, T. Otsuka, and P. Bonche, J. Phys. G **23**, 1267 (1997).
[46] B. Schuetrumpf, P.-G. Reinhard, P. D. Stevenson, A. S. Umar, and J. A. Maruhn, Comput. Phys. Commun. **229**, 211 (2018).
[47] R. Gold, Argonne National Laboratory Report No ANL-6984, 1964; 10.2172/4634295.
[48] M. Travar, V. Piau, A. Göök *et al.*, Phys. Lett. B **817**, 136293 (2021).
[49] G. Scamps, I. Abdurrahman, M. Kafker, A. Bulgac, and I. Stetcu, Phys. Rev. C **108**, L061602 (2023).